Journal of Marine Research, 67, 225–237, 2009

Winter advection of iron can explain the summer phytoplankton bloom that extends 1000 km downstream of the Kerguelen Plateau in the Southern Ocean

by M. M. Mongin[1,2,3], E. R. Abraham[4] and T. W. Trull[1,2,5]

ABSTRACT

The predominantly low-chlorophyll conditions of the Southern Ocean are punctuated by regions of elevated phytoplankton biomass, including a bloom in the Antarctic Circumpolar Current (ACC) that extends for 1000 km downstream of the Kerguelen-Heard islands. Summer-time studies have demonstrated that iron from the islands and intervening shallow plateau (300–600 m) fuels localized production. Whether this supply, or alternatively iron brought to the surface by enhanced mixing in ACC eddies, drives the more extensive downstream bloom has not been addressed. We show that the extent and shape of the downstream bloom can be reproduced by simulating the winter-time spread of a slowly-decaying tracer (iron) from the islands and plateau using a satellite-altimetry based advection scheme. This suggests that mesoscale activity in the ACC plays a minor role in generating the enhanced biomass and emphasizes the importance of shallow bathymetry, large-scale advection, and winter-time observations in understanding the productivity of the Southern Ocean.

1. Introduction

Artificial iron fertilization experiments have shown that the addition of iron into HNLC (High Nutrient Low Chlorophyll) waters enhances phytoplankton productivity (as reviewed by, Boyd *et al.* (2007)). Despite their utility, these experiments have been inconclusive on the large-scale potential ecosystem response and the long-term export of carbon. To understand the response to sustained iron fertilization, comprehensive biogeochemical assessments of naturally fertilized areas have been recently completed, including the KEOPS project above the Kerguelen plateau (Blain *et al.*, 2007), the CROZEX project offshore from the Crozet islands (Pollard *et al.*, 2007), and work in Drake Passage (Hopkinson *et al.*, 2007). Those regions, where natural fertilization occurs over a large scale, offer a better means to explore the impact of increased iron supply on biogeochemical cycles and ecosystems (Boyd, 2007).

The KEOPS (Kerguelen Ocean and Plateau compared Study) projects focused on the Kerguelen plateau region, where Moore and Abbott (2000) reported some of the highest

---

[1] Antarctic Climate and Ecosytems CRC, Hobart, Tasmania 7001, Australia.
[2] CSIRO, Marine and Atmospheric Research, Hobart, Tasmania 7001, Australia.
[3] Corresponding author. ***email: mathieu.mongin@csiro.au***.
[4] Dragonfly, 10 Milne Terrace, Island Bay, Wellington 6023, New Zealand.
[5] Institute of Antarctic and Southern Ocean Studies, University of Tasmania, Hobart, Tasmania 7001, Australia.

values of chlorophyll ever observed in the open Southern Ocean. As seen from space (Fig. 1), a large phytoplankton bloom extends downstream of the archipelago in the ACC (Antarctic Circumpolar Current). The increase in phytoplankton biomass above and around the plateau has been attributed to an increase of iron supply (Blain *et al.*, 2001, 2007; Bucciarelli *et al.*, 2001).

The extent of the phytoplankton bloom, more than a 1000 km downstream of the Kerguelen Island, raises the question of whether iron enrichment from the shelf alone is enough to fertilize the bloom region or whether enhanced vertical mixing in the mesoscale eddies of the ACC is required. In this paper, we show that the high chlorophyll downstream from the Kerguelen-Heard islands and plateau could be sustained by horizontal advection alone. We use a simple horizontal tracer advection scheme, and compare the results with satellite ocean color chlorophyll-*a* observations.

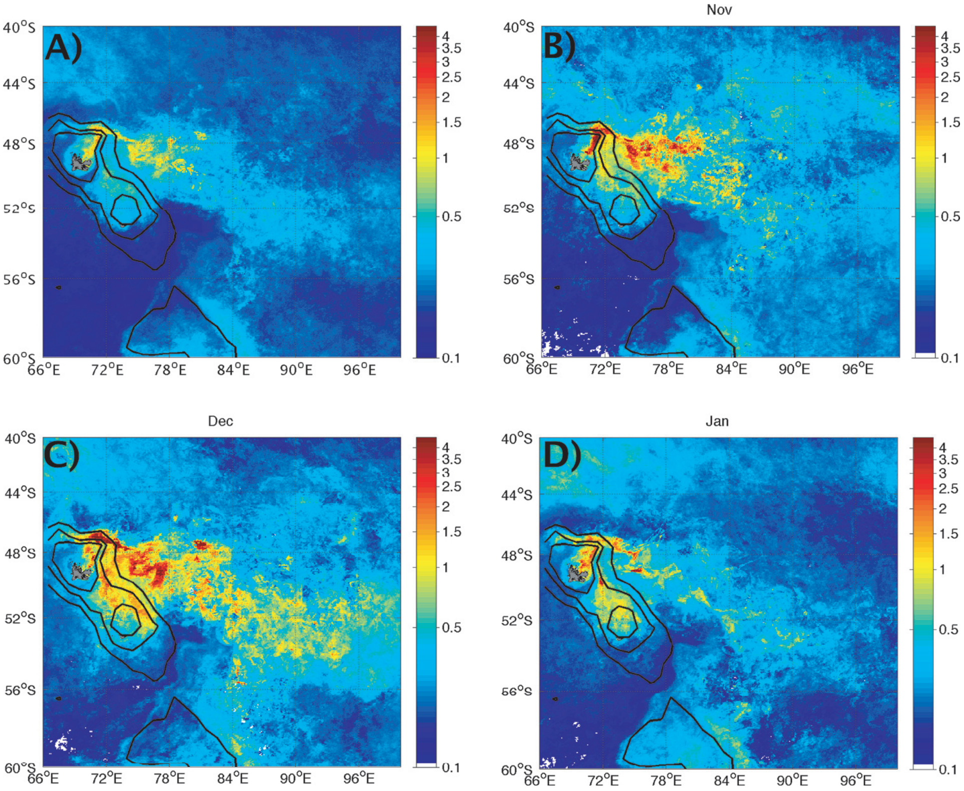

Figure 1. Surface Chlorophyll-*a* climatology (1997–2007) from the MODIS AQUA sensor: A - Annual average, B - November only, C - December only, D - January only. Black lines show the 500 1000 and 2000 m isobaths. Mercator projection.

2. Methods

The Tracer Advection Scheme (TAS) uses the absolute geostrophic velocity field derived from sea surface elevation satellite products (extracted from the merged TOPEX/Poseidon and ERS-1/2 data set at the Archiving Validation and Interpretation of Satellite Data in Oceanography project, AVISO). The mean height field is based on the sum of sea level anomaly (SLA) fields with mean dynamic topography (MDT) estimated from satellite and *in-situ* observations (the MDT product was Rio05, which represents the mean sea surface height above geoid computed on a 7 years period (1993–1999). The AVISO velocity fields were interpolated onto the TAS grid (66°E–100°E with a 1/3° resolution and 40°S–60°S with a 1/6° resolution). Estimates of the distribution of Eddy Kinetic Energy (EKE) were also computed from these velocities (Fig. 2c). The forward trajectory in the velocity field was computed with a 4th order Runge-Kutta integrator and a time step of one day. Turbulent diffusion was not included at a scale smaller than the spatial resolution of the altimetry data. Using Eq. 1 (Hirsch, 1991) we estimated an approximate numerical diffusivity, Dn, from the space (dx or dy) and time (dt) steps used in the scheme and the altimetry-based advective velocities (u and v):

$$Dn = \frac{1}{2} u dx \left[1 - u \left[\frac{dt}{dx} \right] \right] \tag{1}$$

to be ~250 $\mathrm{m}^2\ \mathrm{s}^{-1}$ in both the latitudinal and meridional directions. This is lower than the effective horizontal eddy diffusivity driven by the ACC, which has been estimated to range from ~2500 $\mathrm{m}^2\ \mathrm{s}^{-1}$ north of the Sub-Antarctic Front down to ~500 $\mathrm{m}^2\ \mathrm{s}^{-1}$ south of the Polar Front in this region (Marshall *et al.*, 2006; Stammer, 1997).

To determine the spatial distribution of surface Chlorophyll-*a* (referred to as SCHL hereafter) we used the seven-year annual climatology (2000–2007), the seven-year monthly climatology (2000–2007) or monthly composite of the Level-3 Standard Mapped case 1 Chlorophyll-*a* data provided by the MODIS Project, NASA/Goddard Space Flight Center and GeoEye. The annual climatology (Fig. 1a) removes the small-scale signal and interannual variability, and enables an idealized SCHL bloom to be extracted, the monthly climatology allowed exploration of the seasonal variability, while the monthly composite was used to examine interannual variability. The eastward extension of the bloom was determined either by using the annual climatology (Fig. 1a) or the monthly climatology (using the month of maximum extension, December, Fig. 1c). The elevated SCHL observed south of the Kerguelen bloom (84°E, 57–60°S) is linked to the Banzare Bank recirculation gyre, and we have made no effort to simulate or discuss it in the present study.

To simulate the dispersion of iron, we assumed that its dynamics can be approximated by dispersion and a first order decay rate to parameterize loss, and thus can be represented as a tracer with the following dynamics:

$$\frac{\partial C}{\partial t} = -u \frac{\partial C}{\partial x} - v \frac{\partial C}{\partial y} - \lambda C \tag{2}$$

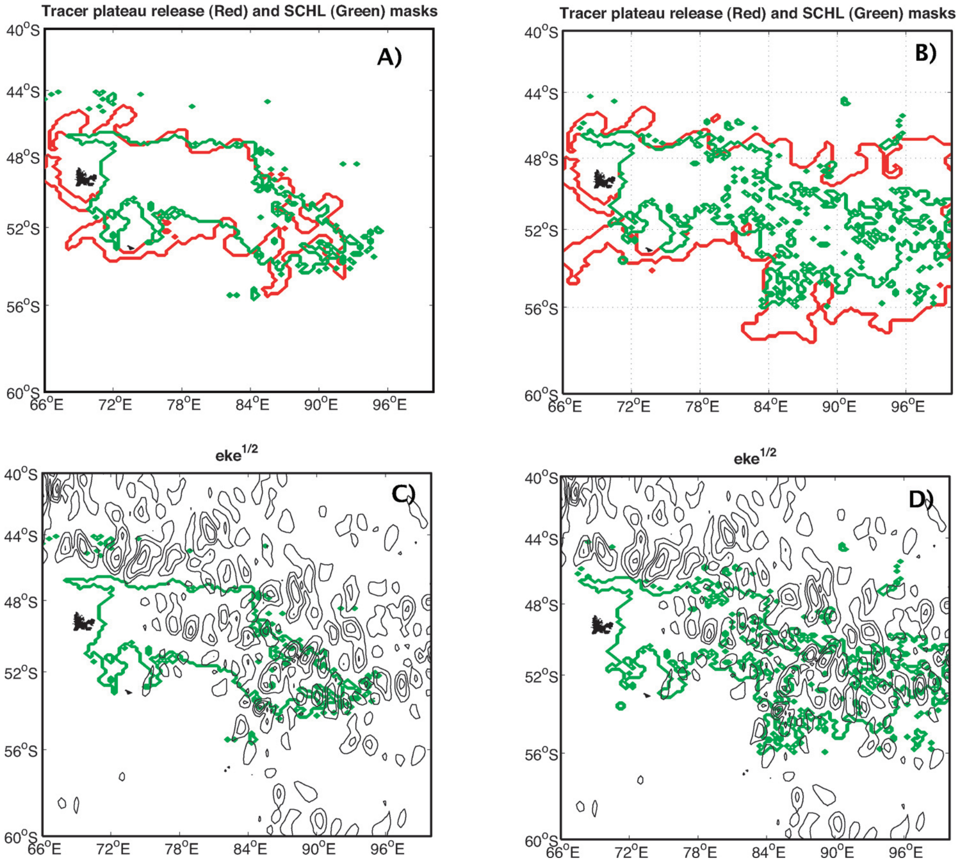

Figure 2. A - Contours of the synthetic tracer (red) at steady state (decay of 1.5% d^{-1}) and the SCHL all months climatology (green; values above the threshold of 0.275 mg m^{-3}). B - Contours of the synthetic tracer (red) at steady state (decay of 0.4% d^{-1}) and the SCHL December only climatology (green; values above the threshold of 0.275 mg m^{-3}). C - Contours of the SCHL all months climatology and eddy kinetic energy field (0.5, 1, 1.5 and 2 $cm^2\ s^{-1}$). D - Contours of the SCHL December only climatology and eddy kinetic energy field (0.5, 1, 1.5 and 2 $cm^2\ s^{-1}$).

where C is the tracer concentration, u and v the horizontal velocities and λ the tracer decay rate (d^{-1}). To simulate supply from the islands and plateau, the tracer concentration was set to 1 at each time step at all shallow bathymetry (depth $<$ 500 m) locations. Off the plateau, a steady state of the tracer distribution is reached after a few months when the source from the shallow sea floor becomes balanced by the tracer decay (see Eq. 2). This ‘tracer decay rate’ is a loss term for the iron supplied from the shelf. As such, it mostly represents scavenging of dissolved iron by particles, as well as biological uptake in surface waters. We ran the model using tracer decay rates ranging from 0% to 10% (d^{-1}). The model was run for one year at a time (from 2000 to 2007) and a similar climatology as the one for the chlorophyll was computed, i.e we calculated a time-varying tracer field and then averaged it.

3. Results

a. Simulating the SCHL plume

By using sea surface elevation to estimate oceanic currents, we only take into account the large-scale flow; the wind derived and tidal flows are not represented. Consequently, we do not expect to reproduce small-scale structures within the SCHL distribution, nor a high-quality representation of the processes close to shore. Offshore, the TAS reproduces remarkably well the general shape of the SCHL plume. Both the annual mean extension (Fig. 2a) and the maximum extension (Fig. 2b) of the phytoplankton bloom can be represented, with a lower decay rate of the tracer providing the best simulation in the maximum extension case (See the discussion about decay rate in the following sections). The sharp bends in the northern part of the plume (47°S, 84°E) are clearly reproduced and suggest a strong interaction with the middle branch of the Sub-Antarctic front [as previously noted by Sokolov and Rintoul (2007)]. Similarly the relatively large bend of SCHL directed toward the south (58°S, 84°E) visible during December (Fig. 2b) is represented in the tracer model when using a low decay rate.

The good representation of those edge patterns is probably due to the higher advection rates that occur in those areas in association with the SAF and PF (Polar Front). In contrast the Eddy Kinetic Energy(EKE) distribution (Fig. 2c,d), which represent area of possible nutrient injection via mesoscale enhanced mixing differs greatly from that of the SCHL bloom, the areas of high kinetic energy do not always correspond to areas of high Chlorophyll with the two patterns being different. This suggest that eddies in the ACC and SAF play a minor role in generating the phytoplankton bloom.

b. Determining the SCHL threshold

To compare the tracer and the SCHL spatial distribution in detail, we first needed to isolate the fertilized SCHL plume from the background level.

Using the studies of Fiala *et al.* (1998); Moore and Abbott (2000), and our own SCHL images, we chose an average background level of SCHL in the Southern Ocean of 0.275 mg Chl*a* m^{-3}. This background value was then removed from the SCHL (Fig. 1a,c) signal to obtain the plume of SCHL resulting from iron fertilization (hereafter referred to as SCHLB, Fig. 2a,b). In parallel, to obtain a continuous tracer plume, without impacting the eastward extension of it, we defined the tracer plume as the area where the tracer concentration was more than 5% of the initial source (with this approximation used only for contouring and masking purpose on Fig. 2a,b).

It is possible to extract a continuous and unique contour delimiting the plume of SCHL when using the annual mean (as in Fig. 2a), but is not possible when using the December climatology (which link with the Banzare bank bloom, and displays a very patchy distribution). We therefore decided to use the annual mean as a reference for the fertilized SCHL plume, keeping in mind that it is the most conservative estimation of the SCHL bloom extension.

c. Steady state and optimum decay rate of the tracer

Because we use different values of the first order decay and run the model for 365-day cycles, we need to assure that a steady state is reached within the year of simulation. We only show the time evolution of the zonal extension of the tracer using the year 2000 model run tracer and not the tracer 2000–2007 climatology, the effect of the interannual variability in the velocity field changes the time required to reach steady state by less than 10 days, which we consider as negligible. Figure 3a shows development of the eastward extension of the plume with time (calculated from the zonal mean between 40°S and 60°S). This extension was inferred at each time step from the longitude at which the tracer concentration is equal to 0.05 (a value which generally provided a continuous contour). This diagnostic was then used to identify the time required to reach steady state, i.e. the quasi-stationary meridional extension. With a decay rate higher than 2%, the steady state is reached in 60 to 120 days, whereas with a value of 1.5% it is reached after 200 days.

The tracer decay rate represents many underlying processes that are poorly constrained. To address this, we ran the TAS 27 times using different decay rates ranging from 0 to 10% per day and looked at the correlation between the tracer (2000–2007 climatology as in Figure 2a) and SCHLB distribution as a function of decay rate (Fig. 3b). We examined correlations that included concentration variations (referred to as standard correlations), and correlations based on just the presence or absence of the tracer or the SCHLB (referred to as masks, for which all the SCHL and tracer value larger than 0.275 or 0.01, 0.05 and 0.1 respectively were set to 1).

The correlation coefficient between the tracer and SCHLB concentrations was maximal for a tracer decay rate of 0.5% d^{-1}, while the correlation coefficient between the SCHLB mask and tracer mask was maximal for a tracer decay rate between .5% d^{-1} (0.1 tracer threshold) and 3% d^{-1} (0.01 tracer threshold).

The rank correlation that describes the relationship between two variables without making any assumptions about their frequency distributions also reached its maximum of 0.68 for a decay rate of 1.5% per day, but cannot be used for evidence for a 1.5% decay rate when compared to a correlation coefficient of 0.64 for 10% decay.

As we were primarily interested in the spatial extension of the plume and not the structure within the plume, we follow the indication given by the mask correlation coefficient and considered a range of tracer decay between 0.4 and 3% per day, use a median value of 1.5% per day to provide the best representation. For representing the December only bloom (Fig. 2b), and to account for the larger bloom, the decay was reduced from 1.5% d^{-1} to 0.4% d^{-1}.

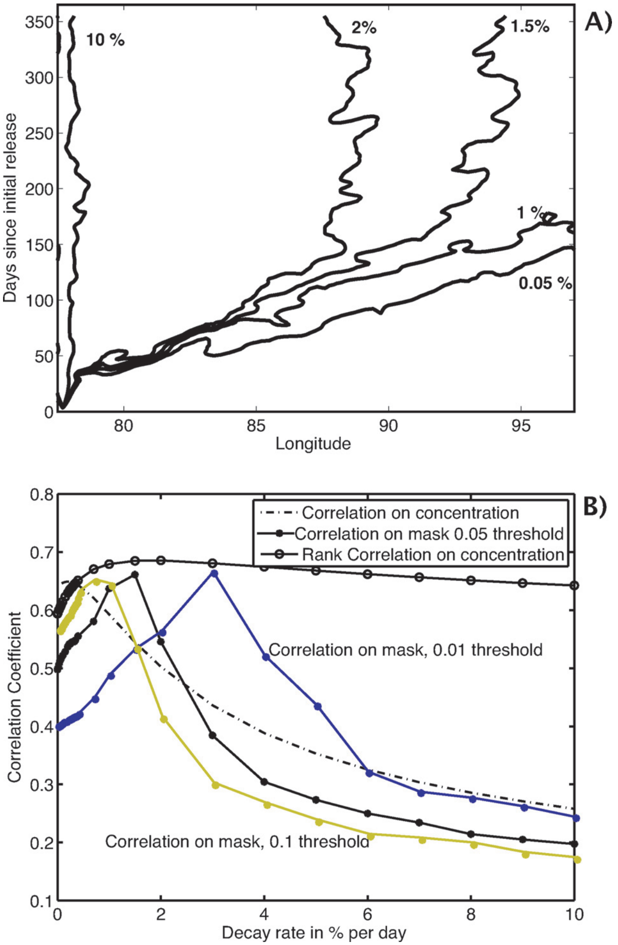

Figure 3. A - Time evolution of the zonal extension of the tracer bloom under different decay rates (using a 0.05 threshold). B - Correlation coefficients between the tracer and SCHL spatial distributions.

4. Discussion

We have shown that a tracer advected from shallow waters over the Kerguelen-Heard Plateau can reproduce the SCHL plume. By looking at the time evolution of the bloom (Fig. 1b,c,d), we see that large changes occur within a few weeks, which is much shorter than the time scale of the advection (∼2–3 months to traverse the model domain). This eliminates the possibility that the plume is caused by advection of the SCHL itself. The development of the bloom may be interpreted as a consequence of the advected iron concentration. Iron is released near the islands and above the plateau during the low-growth winter months and spreads eastwards. When irradiance increases in spring, phytoplankton growth accelerates, producing a bloom that is equivalent in shape to the dispersed iron.

The bloom resulting from natural fertilization is extracted using the climatological annual mean of SCHL, which is the most conservative estimate of the eastward extension of the bloom and hence of the tracer decay rate (1.5% d^{-1}). The extention of the bloom is somewhat larger during December (Fig. 1c), which require a three fold decrease in the decay rate (0.4% d^{-1}).

The dispersion driven by the TAS can also be compared to observations of dissolved Fe. Assuming that the shelf iron concentration ranges between 0.58 and 2.71 nmol m^{-3} (following measurements made by Bucciarelli *et al.* (2001)), the model suggests concentrations at the bloom edge of between 0.03 and 0.13 nmol m^{-3}. This is close to the typical iron concentration of 0.08–0.12 nmol m^{-3} found in most Southern Ocean open waters (Sedwick *et al.*, 2008; Measures and Vink, 2000), and similar to the levels of iron inferred to stimulate production (Boyd *et al.*, 2001). These comparisons must of course be considered with caution, since we have not accounted for change in vertical mixing downstream of the plateau. Addressing this issue is beyond the scope of this study, but would be expected to reduce near-source iron concentrations by dilution, and then at large distances to elevate them by resupply.

The model decay rate represents an annual averaged scavenging rate. Interestingly, this constant removal rate is comparable with the long-term iron turnover rate of 100 days (for a daily export flux of 1%) calculated by Boyd *et al.* (2005) during the FeCycle experiment, and similar to the one used in the Parekh *et al.* (2004) and Moore and Braucher (2008) models of global iron cycling (1.8% d^{-1} and 1.5% d^{-1} respectively). In addition, assuming a 90-day growth season, this fixed 1.5% decay per day would correspond to a rate of 6.1% d^{-1} during the bloom period and almost zero during the rest of the year, comparable with the 5% d^{-1} calculated by Coale *et al.* (2004) for the SoFex experiment. The loss rate also falls in the range of 0.3 and 3% d^{-1} deduced for the SOIREE bloom (Abraham *et al.*, 2000).

Because we use a basic advection scheme and geostrophic current, we need to support the use of this particular scheme by assessing the effective dispersion of the tracer and comparing this with the observation made in the real ocean. The effective eddy diffusivity, which is equivalent to a diffusion coefficient when the tracer transport is phrased as a pure diffusion problem (by converting the advection into diffusion) (Nakamura, 1996), can be used to estimate the dispersion in the TAS. It was calculated using an additional simulation in which the tracer was released at one time step only and had no decay. The resultant tracer distribution was then compared with an analytical solution for one-dimensional diffusion of a point source in a plane sheet (Crank, 1975) [Eq. 2.6]: Overall we use Eq. 3 for determing the concentration distance curve for a given effective diffusivity, and compare those with the one obtained in the model.

$$C(x,t) = \frac{M}{2\sqrt{\pi D t}} e^{\left[-\frac{x^2}{4Dt}\right]} \tag{3}$$

where C is the tracer concentration, M is the amount of tracer released and D is the diffusion coefficient. Figure 4 shows these comparisons for 15 and 150 days after the tracer release, using the zonal mean concentrations. Due to the spatially varying TAS forcing the effective eddy diffusivity is of course not constant over our model domain, so that no single analytical curve fits the TAS concentration curves precisely (as seen in Fig. 4). Nonetheless, the comparisons suggest effective diffusivities ranging between ~2000 $m^2\ s^{-1}$ (15 days after release, close to the source) to 3000 $m^2\ s^{-1}$ (150 days after release, far from the source). This increase of the dispersion rate with time is expected since the tracer reaches zones where the different branches of the ACC rejoin at ~90°E (Park *et al.*, 2008; Sokolov and Rintoul, 2007), resulting in a much higher advection rate, and stronger EKE (Fig. 2b). A similar trend was seen by Karsten and Marshall (2002) with values between 1000 $m^2\ s^{-1}$ and 2500 $m^2\ s^{-1}$ over the plateau and between 2500 $m^2\ s^{-1}$ and 4000 $m^2\ s^{-1}$

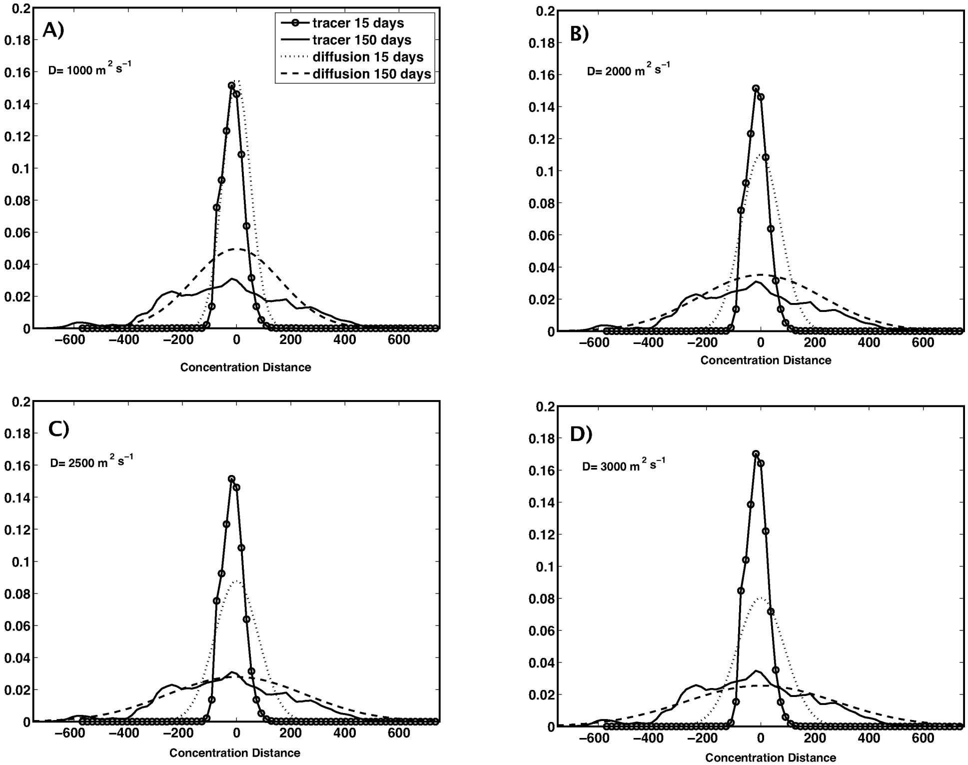

Figure 4. Concentration versus distance curves for the tracer without decay (solid lines) and analytical diffusion equation (dotted lines) for four different values of the diffusion coefficient, and for two times (15 and 50 days) after tracer release. Distances were calculated from the point of maximum concentration (zonally averaged). North is to the right in each panel. A - D $= 1000\ m^2s^{-1}$, B $-$ D $= 2000\ m^2s^{-1}$, C - D $= 2500\ m^2s^{-1}$, D - D $= 3000\ m^2s^{-1}$.

farther east. Using a similar tracer release simulation Marshall *et al.* (2006) reported an effective eddy diffusivity slightly lower than ours, with values between 1500 m^2 s^{-1} and 2000 m^2 s^{-1} at 45°S–50°S. These tests show that, despite its relative simplicity, the TAS is a reasonable tool for analysing horizontal dispersal in the wake of the Kerguelen-Heard Plateau.

The analysis of the SCHL fields for the 2002–2007 period shows that the interannual variability of the bloom is quite large, both in term of covered area and maximum observed concentrations. These variations could arise from changes in the magnitude of iron supply from the islands in plateau, for example as a result of varying depths of mixing in winter, or from differences in the subsequent downstream dispersion of the iron. Diagnosing the detailed origins of interannual variability is beyond the scope of this study, and is likely to require additional observations, but comparison of the two years, 2003 and 2004, with the greatest differences in the extent of the downstream phytoplankton bloom does provide some insights. As shown in Figure 5, 2003 was a year with relatively high zonal velocities, and 2004 a year with relatively low zonal velocities, and the extent of the blooms in those years do show that higher velocities produced a more extensive downstream bloom. In 2003, the bloom was quite large in November, with SCHL value well above 2.5 mg SCHL m^{-3} and extended as far as 98°E by December. In contrast, in November and December 2004 the bloom did not extend beyond approximately 86°E and was weaker in intensity.

These results suggest that at least some aspects of interannual variability can be understood as the result of variations in advection, but also emphasize that a fuller understanding will require more detailed knowledge of the processes that supply iron, engender phytoplankton growth, and then retain or remove it from the surface water ecosystem. In short, a complete biogeochemical model coupled with a physical model of the Kerguelen plateau will be needed to further investigate these issues.

5. Conclusion

This study suggests that advection of iron from shallow waters enhances Southern Ocean primary production over a very large area, and that this effect alone may explain the large phytoplankton bloom that forms downstream from the Kerguelen-Heard plateau, without the need to invoke an important role for iron supply from below in association with eddy activity. Looking at iron concentrations in the wake of the Kerguelen Island, Bucciarelli *et al.* (2001) had already suggested that the increase in productivity could be due to nutrients being transported far offshore. Our results support this hypothesis and suggest that it extends for $\sim$1000 km, and that mildly elevated iron concentrations (around 0.3–0.4 nmol m^3) should be observed in this area in winter. In summary, a low decay rate of the iron, a low threshold for the phytoplankton response, and predominance of lateral transport over vertical mixing combine to make possible the development of one of the largest phytoplankton blooms in the Southern Ocean.

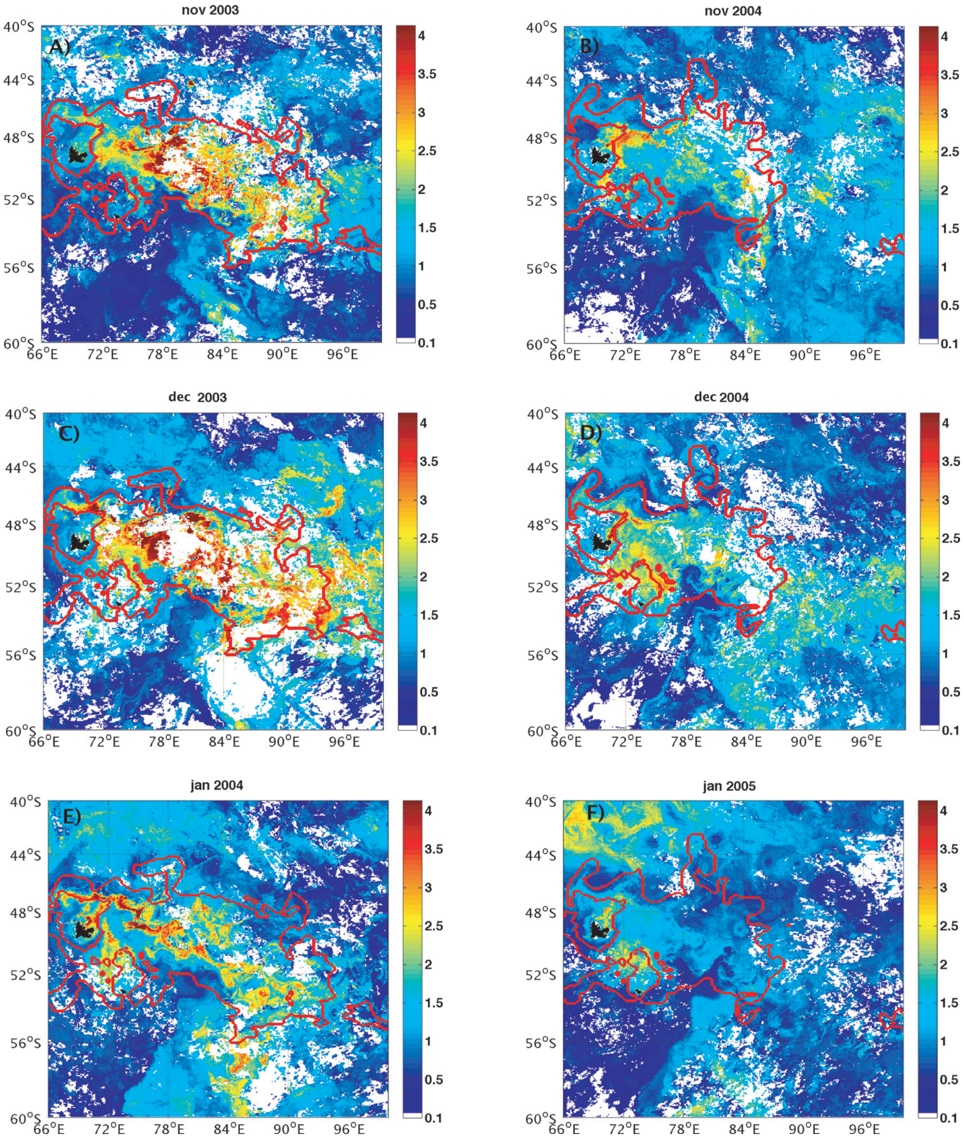

Figure 5. Surface Chlorophyll-*a* Monthly Composite from the MODIS AQUA sensor and Contour of the synthetic tracer (red) at steady state. A - November 2003 SCHL and contour of the synthetic tracer at steady state in 2003 (decay of 1.5% d^{-1}). B - November 2004 SCHL and contour of the synthetic tracer at steady state in 2004 (decay of 1.5% d^{-1}). C - December 2003 SCHL and contour of the synthetic tracer at steady state in 2003 (decay of 1.5% d^{-1}). D - December 2004 SCHL and contour of the synthetic tracer at steady state in 2004 (decay of 1.5% d^{-1}). E - January 2003 SCHL and contour of the synthetic tracer at steady state in 2003 (decay of 1.5% d^{-1}). F - January 2004 SCHL and contour of the synthetic tracer at steady state in 2004 (decay of 1.5% d^{-1}).

Acknowledgments. We thank Richard Matear, Andrew Bowie, and Matt Charette for insightful discussions, and David Griffins and Steve Rintoul for constructive internal reviews. This work was funded by the Australian Commonwealth Cooperative Research Centres Program.

REFERENCES

Abraham, E., C. Law, P. Boyd, S. Lavender, M. Maldonado, and A. Bowie. 2000. Importance of stirring in the development of an iron-fertilized phytoplankton bloom. Nature, *407*, 727–730.

Blain, S., B. Queguiner, L. Armand, S. Belviso, B. Bombled, L. Bopp, A. Bowie, C. Brunet, C. Brussaard, F. Carlotti, U. Christaki, A. Corbiere, I. Durand, F. Ebersbach, J.-L. Fuda, N. Garcia, L. Gerringa, B. Griffiths, C. Guigue, C. Guillerm, S. Jacquet, C. Jeandel, P. Laan, D. Lefevre, C. Lo Monaco, A. Malits, J. Mosseri, I. Obernosterer, Y.-H. Park, M. Picheral, P. Pondaven, T. Remenyi, V. Sandroni, G. Sarthou, N. Savoye, L. Scouarnec, M. Souhaut, D. Thuiller, K. Timmermans, T. Trull, J. Uitz, P. van Beek, M. Veldhuis, D. Vincent, E. Viollier, L. Vong, and T. Wagener. 2007. Effect of natural iron fertilization on carbon sequestration in the Southern Ocean. Nature, *446*, 1070–U1. doi: 10.1038/nature05700.

Blain, S., P. Treguer, S. Belviso, E. Bucciarelli, M. Denis, S. Desabre, M. Fiala, V. Jezequel, J. Le Fevre, P. Mayzaud, J. Marty, and S. Razouls. 2001. A biogeochemical study of the island mass effect in the context of the iron hypothesis: Kerguelen Islands, Southern Ocean. Deep-Sea Res. I, *48*, 163–187.

Boyd, P. W. 2007. Biogeochemistry – Iron findings. Nature, *446*, 989–991. doi: 10.1038/446989a.

Boyd, P., A. Crossley, G. DiTullio, F. Griffiths, D. Hutchins, B. Queguiner, P. Sedwick, and T. Trull. 2001. Control of phytoplankton growth by iron supply and irradiance in the subantarctic Southern Ocean: Experimental results from the SAZ Project. J. Geophys. Res., Oceans, *106*, 31573–31583.

Boyd, P. W., T. Jickells, C. S. Law, S. Blain, E. A. Boyle, K. O. Buesseler, K. H. Coale, J. J. Cullen, H. J. W. de Baar, M. Follows, M. Harvey, C. Lancelot, M. Levasseur, N. P. J. Owens, R. Pollard, R. B. Rivkin, J. Sarmiento, V. Schoemann, V. Smetacek, S. Takeda, A. Tsuda, S. Turner, and A. J. Watson. 2007. Mesoscale iron enrichment experiments 1993–2005: Synthesis and future directions. Science, *315*, 612–617. doi: 10.1126/Science.1131669.

Boyd, P., C. Law, D. Hutchins, E. Abraham, P. Croot, M. Ellwood, R. Frew, M. Hadfield, J. Hall, S. Handy, C. Hare, J. Higgins, P. Hill, K. Hunter, K. LeBlanc, M. Maldonado, R. McKay, C. Mioni, M. Oliver, S. Pickmere, M. Pinkerton, K. Safi, S. Sander, S. Sanudo-Wilhelmy, M. Smith, R. Strzepek, A. Tovar-Sanchez, and S. Wilhelm. 2005. FeCycle: Attempting an iron biogeochemical budget from a mesoscale SF6 tracer experiment in unperturbed low iron waters. Global Biogeochem. Cycles, *19*. doi: 10.1029/2005GB002494.

Bucciarelli, E., S. Blain, and P. Treguer. 2001. Iron and manganese in the wake of the Kerguelen Islands (Southern Ocean). Mar. Chem., *73*, 21–36.

Coale, K., K. Johnson, F. Chavez, K. Buesseler, R. Barber, M. Brzezinski, W. Cochlan, F. Millero, P. Falkowski, J. Bauer, R. Wanninkhof, R. Kudela, M. Altabet, B. Hales, T. Takahashi, M. Landry, R. Bidigare, X. Wang, Z. Chase, P. Strutton, G. Friederich, M. Gorbunov, V. Lance, A. Hilting, M. Hiscock, M. Demarest, W. Hiscock, K. Sullivan, R. Tanner, SJ Gordon, C. Hunter, V. Elrod, S. Fitzwater, J. Jones, S. Tozzi, M. Koblizek, A. Roberts, J. Herndon, J. Brewster, N. Ladizinsky, G. Smith, D. Cooper, D. Timothy, S. Brown, K. Selph, C. Sheridan, B. Twining, and Z. Johnson. 2004. Southern Ocean iron enrichment experiment: Carbon cycling in high- and low-Si waters. Science, *304*, 408–414.

Crank, J. 1975. The Mathematics of Diffusion, Oxford University Press, 2nd ed., 230–238.

Fiala, M., E. Kopczynska, C. Jeandel, L. Oriol, and G. Vetion. 1998. Seasonal and interannual variability of size-fractionated phytoplankton biomass and community structure at station Kerfix, off the Kerguelen Islands, Antarctica. J. Plank. Res., *20*, 1341–1356.

Hirsch, C. 1991. Numerical Computation of Internal and External Flows, John Wiley and Sons Ltd., 647 pp.

Hopkinson, B. M., G. Mitchell, R. A. Reynolds, H. Wang, K. E. Selph, C. I. Measures, C. D. Hewes, O. Holm-Hansen, and K. A. Barbeau. 2007. Iron limitation across chlorophyll gradients in the southern Drake Passage: Phytoplankton responses to iron addition and photosynthetic indicators of iron stress. Limnol. Oceanogr., *52*, 2540–2554.

Karsten, R. and J. Marshall. 2002. Constructing the residual circulation of the ACC from observations. J. Phys. Oceanogr., *32*, 3315–3327.

Marshall, J., E. Shuckburgh, H. Jones, and C. Hill. 2006. Estimates and implications of surface eddy diffusivity in the Southern Ocean derived from tracer transport. J. Phys. Oceanogr., *36*, 1806–1821.

Measures, C. and S. Vink. 2000. On the use of dissolved aluminum in surface waters to estimate dust deposition to the ocean. Global Biogeochem. Cycles, *14*, 317–327.

Moore, J. and M. Abbott. 2000. Phytoplankton chlorophyll distributions and primary production in the Southern Ocean. J. Geophys. Res., Oceans, *105*, 28709–28722.

Moore, J. K. and O. Braucher. 2008. Sedimentary and mineral dust sources of dissolved iron to the world ocean. Biogeosciences, *5*, 631–656.

Nakamura, N. 1996. Two-dimensional mixing, edge formation, and permeability diagnosed in an area coordinate. J. Atmos. Sci., *53*, 1524–1537.

Parekh, P., M. Follows, and E. Boyle. 2004. Modeling the global ocean iron cycle. Global Biogeochem. Cycles, *18*. doi: 10.1029/2003GB002061.

Park, Y.-H., F. Roquet, I. Durand, and J.-L. Fuda. 2008. Large-scale circulation over and around the Northern Kerguelen Plateau. Deep-Sea Res. II, *55*, 566–581. doi: 10.1016/j.dsr2.2007.12.030.

Pollard, R., R. Sanders, M. Lucas, and P. Statham. 2007. The crozet natural iron bloom and EXport experiment (CROZEX). Deep-Sea Res. II, *54*, 1905–1914. doi: 10.1016/j.dsr2.2007.07.023.

Sedwick, P. N., A. R. Bowie, and T. W. Trull. 2008. Dissolved iron in the Australian sector of the Southern Ocean (CLIVAR SR3 section): Meridional and seasonal trends. Deep-Sea Res. I, *55*, 911–925. doi: 10.1016/j.dsr.2008.03.011.

Sokolov, S. and S. R. Rintoul. 2007. On the relationship between fronts of the Antarctic Circumpolar Current and surface chlorophyll concentrations in the Southern Ocean. J. Geophys. Res., Oceans, *112*. doi: 10.1029/2006JC004072.

Stammer, D. 1997. Global characteristics of ocean variability estimated from regional TOPEX/POSEIDON altimeter measurements. J. Phys. Oceanogr., *27*, 1743–1769.

Received: *4 December, 2008*; revised: *24 March, 2009*.